# Contribution of the Politecnico di Milano to the FUMEX-III Project

**Lelio Luzzi[*,1], Giovanni Pastore[1], and Paul Van Uffelen[2]**

[1]*Politecnico di Milano, Department of Energy, Nuclear Engineering Division (CeSNEF), Italy*
[2]*European Commission, Joint Research Centre, Institute for Transuranium Elements, Germany*

**November 2011**


[*]Corresponding author
E-mail address: lelio.luzzi@polimi.it

(This page has been intentionally left blank)

## FOREWORD

In nuclear reactors, irradiation continuously alter the thermal, mechanical, and chemical properties of nuclear fuels (Olander 1976). To assure the safe and economic operation of the nuclear fuel rods in all the operation conditions, there is a need for fuel characterization and optimization through an integrated theoretical, experimental, and computational approach. The aim of computational fuel modelling is to predict the changes in properties and evaluate the thermo-mechanical behaviour of the fuel rods during the life in the reactor. For this purpose, increasingly complex fuel performance codes are developed, which include physical models of the processes taking place in the fuel rods during irradiation (Aybar and Ortego 2005).

In this framework, international benchmark exercises on fuel modelling are of high importance for the development of fuel performance codes, since they provide the possibility for cross-comparison and complementary validation of a large number of codes involved. Three such exercises were organized during the last 3 decades: D-COM in the mid 80's (Misfeldt 1983), and the Coordinated Research Projects (CRPs) FUMEX-I (1993-1996) (Chantoin et al. 1997) and FUMEX-II (2002-2006) (Killeen et al. 2007, IAEA 2011). In extending the previous CRPs on the subject of improving the predictive capabilities of fuel performance codes for extended burn-up and transient conditions, the focus of the CRP FUMEX-III (2008-2012) is on the topics of fission gas release, pellet-cladding interaction (PCI) and dimensional changes (Killeen et al. 2009).

The TRANSURANUS fuel performance code (Lassmann 1992, Lassmann 2001) is presently available at the Politecnico di Milano (POLIMI). Based on the assumption of axial-symmetric cylindrical rod and the superposition of a one-dimensional radial and axial description (1½D approach), the mechanical-mathematical framework of TRANSURANUS allows to analyze, at reasonable computer cost, the integral fuel rod during a complicated, long power history. TRANSURANUS is applied for design as well as for licensing of nuclear fuel, and is therefore used by research centres, universities, industrial partners and nuclear safety authorities. Moreover, TRANSURANUS is featured by a flexible structure into which physical models can easily be incorporated. A review of the validation of the code is given in (Van Uffelen et al. 2007).

In line with the specific research objectives of FUMEX-III, a primary interest of POLIMI within research on computational fuel modelling lies in the analysis of the behaviour of LWR-$UO_2$ fuel rods during both normal reactor operation and transients. According to the original POLIMI proposal (Luzzi 2008), the main topic of interest of POLIMI in the frame of FUMEX-III was the modelling of PCI, with the aim of predicting the PCI failure thresholds by means of the TRANSURANUS code. However, subsequent assessments of the prediction capability of TRANSURANUS (Pastore et al. 2009a, Pastore et al. 2009b) pointed out that the incorporation of new physical models in the code, with the aim of improving the description of the integral fuel rod behaviour under power transient and pellet-cladding mechanical interaction (PCMI) conditions, is a prerequisite for an accurate modelling of PCI. In particular, developments are needed of the modelling of the fuel swelling due to fission gas build-up (fission gas swelling). In the current version of the TRANSURANUS code, the fission gas swelling rate is described by means of an empirical correlation and neglected under PCMI conditions (due to the lack of a description of the process dependence on the fuel stress state). Moreover, some room for improvement was noticed for the treatment of fission gas release (FGR), which is physically coupled with the fission gas swelling.

On this basis, a new physics-based model of fission gas swelling and release for the TRANSURANUS code has been recently developed in the frame of a collaboration between the POLIMI and the ITU (European Commission, Joint Research Centre, Institute for Transuranium Elements, Karlsruhe, Germany). The model calculates the fission gas swelling and release through a

physical description of the underlying microscopic processes, consistently considering the coupling between the two processes as well as their dependence on the fuel stress state.

The developed model has been firstly implemented as stand-alone version, namely, a computer program has been set up, which receives the fuel fabrication data, temperature, hydrostatic stress and specific power as input and performs the model calculations for a single point in the fuel. The application of the stand-alone version to the analysis of power-ramped AGR-$UO_2$ fuel has allowed a first verification of the model through comparison with experimental data of local fission gas swelling. Subsequently, the model has been incorporated in the TRANSURANUS code and applied to the integral analysis of LWR-$UO_2$ fuel rods under both normal operation and transient reactor conditions, allowing a first assessment of the predictions against experimental data of FGR.

This report gives an account of the present state of development, implementation and validation in the TRANSURANUS code of the new model of fission gas swelling and release, with focus on the application in the frame of FUMEX-III. In section 1, a description of the model is given and the stand-alone version calculations are discussed. In section 2, the first results obtained by applying the model within the TRANSURANUS code are presented, including those of some priority cases of FUMEX-III. Despite the encouraging results, the work is still continuing. The conclusions and perspectives are outlined in the last section.

**CONTENTS**

(This page has been intentionally left blank)

## ACKNOWLEDGEMENTS

This work has been carried out in the framework of a collaboration between the Politecnico di Milano (Department of Energy, Nuclear Engineering Division, Milan, Italy) and the JRC-ITU (European Commission, Joint Research Centre, Institute for Transuranium Elements, Karlsruhe, Germany). L. Luzzi and G. Pastore gratefully acknowledge the TRANSURANUS Developers Team at the ITU for the fruitful collaboration. A special thank is due to Prof. Dr. Klaus Lassmann for his interest and scientific support.

(This page has been intentionally left blank)

## NOMENCLATURE

Latin symbols

| | |
|---|---|
| $a$ | Parameter of the MATPRO swelling model FSWELL [(at%)$^{-1}$] |
| $A_{gp}$ | Projected area of inter-granular gas pores [m$^3$] |
| $b$ | Irradiation-induced resolution parameter [s$^{-1}$] |
| $b_{VdW}$ | Van der Waals' volume of a fission gas atom [m$^3$·(at.)$^{-1}$] |
| $c$ | Parameter of the MATPRO swelling model FSWELL [(at%)$^{-1}$] |
| $bu$ | Burn-up [at%] |
| $C_b$ | Concentration of intra-granular gas residing in bubbles [(at.)·m$^{-3}$] |
| $C_{gb}$ | Concentration of gas at the grain boundaries [(at.)·m$^{-2}$] |
| $C_s$ | Concentration of intra-granular gas existing as single atoms [(at.)·m$^{-3}$] |
| $C_t$ | Concentration of intra-granular gas (single atoms + bubbles) [(at.)·m$^{-3}$] |
| $D_{eff}$ | Effective intra-granular gas diffusion coefficient [m$^2$·s$^{-1}$] |
| $D_{gb}$ | Grain-boundary vacancy diffusion coefficient [m$^2$·s$^{-1}$] |
| $D_s$ | Intra-granular diffusion coefficient of single gas atoms [m$^2$·s$^{-1}$] |
| $F$ | Fission rate density [(fiss.)·m$^{-3}$·s$^{-1}$] |
| $F_c$ | Fraction of grain boundary covered by gas pores (fractional coverage) [/] |
| $g$ | Trapping parameter [s$^{-1}$] |
| $k$ | Boltzmann constant [J/K] |
| $l_f$ | Length of a fission fragment track [m] |
| $m$ | Number of fission gas atoms contained in an intra-granular bubble [(at.)] |
| $n_{fgr}$ | Number of fission gas atoms released into the fuel rod free volumes [(at.)] |
| $n_g$ | Number of fission gas atoms per inter-granular gas pore [(at.)] |
| $n_v$ | Number of vacancies per inter-granular gas pore [(vac.)] |
| $N_b$ | Density of intra-granular bubbles [(bub.)·m$^{-3}$] |
| $N_{gp}$ | Density of inter-granular gas pores [(por.)·m$^{-2}$] |
| $p$ | Gas pressure in the inter-granular gas pores [Pa] |
| $r$ | Radial co-ordinate in the spherical grain [m] |
| $R$ | Specific power [W·g$^{-1}$] |
| $R_b$ | Radius of intra-granular bubbles [m] |
| $R_{gp}$ | Radius of curvature of inter-granular gas pores [m] |
| $r_{gr}$ | Grain radius [m] |
| $t$ | Time [s] |
| $V_{gp}$ | Volume of inter-granular gas pores [m$^3$] |
| $Z_0$ | Radius of influence of a fission fragment track [m] |

Greek symbols

| | |
|---|---|
| $\beta$ | Fission gas generation rate [(at.)·m$^{-3}$·s$^{-1}$] |
| $\gamma$ | $UO_2$/gas specific surface energy [J·m$^{-2}$] |
| $\delta_{gb}$ | Thickness of the diffusion layer in the grain boundary [m] |
| $\Delta(\Delta V/V)_{gas}$ | Increment of fractional volume of fission gas swelling during a time step [/] |
| $(\Delta V/V)_{gb}$ | Fractional volume of intra-granular fission gas swelling [/] |
| $(\Delta V/V)_{gr}$ | Fractional volume of grain-boundary fission gas swelling [/] |
| $\Delta bu$ | Burn-up increment during a time step [at%] |
| $\Delta t$ | Time step [s] |
| $\varepsilon$ | Number of vacancies per fission gas atom in the inter-granular gas pores [/] |
| $\theta$ | Semi-dihedral angle of the inter-granular gas pores [°] |
| $\sigma_h$ | Hydrostatic stress [Pa] |
| $\Omega$ | Atomic volume of gas in the intra-granular bubbles [m$^3$] |
| $\Omega_{gb}$ | Atomic/vacancy volume in the inter-granular gas pores [m$^3$] |

Acronyms

| | |
|---|---|
| AGR | Advanced Gas cooled Reactor |
| CeSNEF | Centro Studi Nucleari "Enrico Fermi" |
| CRP | Coordinated Research Project |
| FGR | Fission Gas Release |
| HBS | High Burn-up Structure |
| IFPE | International Fuel Performance Experiments |
| ITU | Institute for Transuranium Elements |
| BWR | Boiling Water Reactor |
| LWR | Light Water Reactor |
| MOX | Mixed OXide |
| PWR | Pressurized Water Reactor |
| PCI | Pellet-Cladding Interaction |
| PCMI | Pellet-Cladding Mechanical Interaction |
| PIE | Post-Irradiation Examinations |
| POLIMI | Politecnico di Milano |
| RTL | Ramp Terminal Level |
| SEM | Scanning Electron Microscopy |
| TD | Theoretical Density |
| TEM | Transmission Electron Microscopy |

# 1. MODEL DESCRIPTION

## 1.1 Introduction

Processes such as generation, diffusion, accumulation and release of the fission gases xenon and krypton have a strong impact on the fuel rod performance. On the one hand, the fission gases generated in the fuel tend to accumulate in bubbles and gas pores as a consequence of their extremely low solubility, decreasing the heat transfer and possibly leading to overheating of the fuel and local melting. On the other hand, growth and coalescence of bubbles and gas pores cause progressive fuel swelling, which may give rise to enhanced pellet-cladding mechanical interaction and cladding failure. Likewise, the release of a fraction of the generated gas into the free volumes of the fuel rod (fission gas release – FGR) causes pressure build-up and thermal conductivity degradation of the rod filling gas. Consequently, the fuel temperature increases, which under certain circumstances may lead to higher FGR until the rod fails due to cladding ballooning and cladding burst. The effects of fission gas swelling and release as potential design limitation factors can be particularly marked at high burn-up and during reactor transients (Kashibe et al. 1993, Mogensen et al. 1985). Consequently, efficient models of fission gas swelling and release are to be incorporated in fuel performance codes for a suitable description of the fuel rod behaviour under different reactor operation conditions.

In outline, the main processes that control the kinetics of fission gas swelling and release to be modelled in fuel rod performance calculations, are the following. After nucleation in the fuel grains, bubbles grow by collecting gas by single atom diffusion, giving rise to intra-granular swelling. Simultaneously, gas diffuses to the grain boundaries bringing about the formation and growth of inter-granular gas pores and the related grain-boundary swelling. Inter-granular gas pores eventually interlink and form paths for FGR. Diffusion is believed to be always dominant over all the other mechanisms of FGR (e.g., recoil and knock out, release from the high burn-up structure at the rim of the pellet) (Lösönen, 2000, Lösönen 2002).

In the current version of TRANSURANUS, the fission gas swelling and release are described by two distinct models. In particular, the FGR is calculated by means of the solution of the intra-granular gas diffusion equation in an equivalent spherical grain and an empirical saturation gas concentration at the grain boundaries. The fuel deformation due to fission gas swelling is calculated as a function of the burn-up and temperature by means of an empirical correlation. Such a treatment of the fission gas behaviour has advantages in terms of simplicity and, consequently, of speed of calculation. On the other hand, the applicability of empirical models is limited to a regime where experimental data is available.

The attempt of this work is to develop and incorporate in the TRANSURANUS code a new model, which describes the fission gas swelling and release in $UO_2$ fuel as inherently coupled phenomena, on a physical basis. The model is as simple as is consistent with reasonable computational cost and with the uncertainties involved in integral fuel rod analysis, while taking into account the main observed dependencies of the phenomena through a description of the underlying microscopic processes. In particular, the formation and growth of gas bubbles and pores is modelled along with coalescence and inter-linkage of the inter-granular gas pores. The dependence of the phenomena on the hydrostatic stress in the fuel, acting to inhibit both the fission gas swelling and release by compression of the inter-granular gas pores (e.g., (Kashibe and Une 1997)), is considered.

Hereinafter, an outline is given of the models of fission gas swelling and release available in the current version of the TRANSURANUS code. Subsequently, the new proposed model is briefly described, both the intra-granular module (subsection 1.2) and the grain-boundary module (subsection 1.3). Then, the application of the stand-alone model for the simulation of irradiation

experiments from the IFPE (International Fuel Performance Experiments) database (Sartori et al. 2010), and its verification through comparison with experimental data of local grain boundary swelling, is discussed (subsection 1.4).

### *1.1.1 Modelling of fission gas swelling in the current version of the TRANSURANUS code*

The TRANSURANUS standard model for swelling of LWR-oxide fuel (Lassmann et al. 2011) is based on the MATPRO swelling model FSWELL (MATPRO 1979), which calculates the fractional volume changes in the fuel due to the build-up of solid fission products and fission gases during irradiation. In particular, the correlation for the fission gas swelling included in FSWELL is

$$\Delta\left(\frac{\Delta V}{V}\right)_{gas} = a(T)\,exp\left(-c\cdot bu\right)\Delta bu \quad , \tag{1.1}$$

where $\Delta(\Delta V/V)_{gas}$ [/] is the increment of fractional volume fission gas swelling during a time step, $bu$ [at%] is the burn-up, $\Delta bu$ is the burn-up increment during a time step, and $a$, $c$ [(at%)$^{-1}$] are empirical parameters. Moreover, $\Delta(\Delta V/V)_{gas}=0$ is considered when contact pressure arises between pellets and cladding (PCMI conditions).

Taking into account and quantifying the influence of the hydrostatic stress on the fission gas swelling is still an open issue in computational fuel modelling. In fact, the hydrostatic stress is often neglected in swelling models adopted in fuel performance codes, or a value is used, which is constant and uniform (Cacuci 2010).

### *1.1.2 Modelling of fission gas release in the current version of the TRANSURANUS code*

The TRANSURANUS model for FGR in LWR-oxide fuel (Lassmann et al. 2011) basically consists of two parts:

1. Solution of the equation describing the intra-granular diffusion of fission gas.
2. Modelling of the interlinkage condition of the inter-granular gas pores.

As concerns the first part, the diffusion equation describing the time evolution of the concentration of gas generated uniformly at a rate $\beta$ [(at.)·m$^{-3}$·s$^{-1}$] within a spherical grain is

$$\frac{\partial C_t}{\partial t} = D_{eff}\,\frac{1}{r^2}\frac{\partial}{\partial r}\left(r^2\,\frac{\partial C_t}{\partial r}\right) + \beta\,, \tag{1.2}$$

where $C_t$ [(at.)·m$^{-3}$] is the intra-granular gas concentration, $t$ [s] is the time, $r$ [m] is the radial co-ordinate in the spherical grain, and $D_{eff}$ [m$^2$·s$^{-1}$] is the effective diffusion coefficient of fission gas atoms in presence of intra-granular bubbles (see subsection 1.2 for further details). Efficient algorithms are implemented in the TRANSURANUS code for the numerical solution of Eq. (1.2) (Lassmann and Benk 2000), allowing the rate of gas transport to the grain boundaries to be evaluated. The standard TRANSURANUS option for the calculation of $D_{eff}$ is the correlation of Matzke (1980),

$$D_{eff} = 5\cdot 10^{-8}\,exp\left(-40262/T\right), \tag{1.3}$$

where $T$ [K] is the temperature. The role of grain growth in contributing to the gas transport to the grain boundaries (*grain boundary sweeping* effect) is also taken into account (not described here for brevity, details can be found in (Lassmann et al. 2011)).

As concerns the second part, the interlinkage condition of the gas pores at the grain boundaries is represented by the concept of grain boundary saturation. It is assumed that, when a specific empirical threshold is reached of the inter-granular gas concentration, $C_{gb}$ [(at.)·m$^{-2}$], a network of interconnected bubbles has formed, and the gas released to the grain boundaries is also released to the free volumes in the fuel rod. As standard TRANSURANUS option, the threshold concentration is

$$C_{gb} = 6.022 \cdot 10^{19} \text{ (at.)} \cdot \text{m}^{-2}. \qquad (1.4)$$

In addition to the standard option, an alternative treatment is available in the TRANSURANUS code, which is specific for the simulation of power transients. In fact, enhancement of FGR is expected during rapid power changes due to the pellet micro-cracking that means new paths for the release of fission gas (burst release). To describe this effect, a model has been developed at the ITU, which considers a complete release of the gas inventory at the grain boundaries when empirical conditions defining the transient are fulfilled (Van Uffelen et al. 2008). This transient FGR model, which is based on that of Koo et al. (1999) and will be referred to as *ITU model* in this report, provides improvements in the FGR predictions for ramp-tested fuel rods (e.g., Van Uffelen et al. 2008, Pastore et al. 2009b).

Finally, simple empirical models are included in TRANSURANUS for calculating the contributions to FGR due to the phenomena of athermal release and high burn-up structure (HBS) release, which are not described here for brevity. Details can be found in (Lassmann et al. 2011).

## 1.2 Intra-granular module

The proposed model of fission gas swelling and release for the TRANSURANUS code includes an intra-granular module, which describes both the intra-granular fission gas diffusion and the intra-granular fission gas swelling. The approach is pragmatic and simple, in view of the computational cost requirements and the uncertainties involved in integral fuel rod analysis. The basic features of this module are presented in the following.

### *1.2.1 Intra-granular fission gas diffusion*

A description of the diffusion of fission gas within the fuel grains (intra-granular fission gas diffusion) during irradiation, which is widely used in computational fuel modelling, is the formulation of Speight (Speight 1969). The formulation of Speight is based on the assumptions that (i) single gas atoms diffuse through the crystal lattice with a single atom diffusion coefficient, $D_s$ [m$^2$·s$^{-1}$], (ii) gas bubbles are immobile, (iii) gas atoms are absorbed into bubbles at a rate $g$ [s$^{-1}$] (trapping parameter), (iv) gas atoms are knocked back from bubbles into the lattice at a rate $b$ [s$^{-1}$] (irradiation-induced resolution parameter), (v) the parameters $g$ and $b$ are considered as spatially independent within a grain and slowly varying in time, and (vi) bubbles are effectively saturated (quasi-stationary approach), giving

$$\frac{C_s}{C_b} = \frac{b}{g}, \qquad (1.5)$$

where $C_s$ [(at.)·m$^{-3}$] is the concentration of intra-granular gas existing as single atoms, and $C_b$ [(at.)·m$^{-3}$] is the concentration of intra-granular gas residing in bubbles.

Under the above assumptions, the intra-granular gas diffusion in presence of bubbles may be evaluated by solving a single diffusion equation, instead of a diffusion equation coupled with an equation for the gas balance in the bubbles. According to the formulation of Speight, the diffusion equation describing the time evolution of the concentration of gas generated uniformly at a rate $\beta$ within a spherical grain is

$$\frac{\partial C_t}{\partial t} = \frac{b}{b+g} D_s \frac{1}{r^2} \frac{\partial}{\partial r}\left( r^2 \frac{\partial C_t}{\partial r} \right) + \beta , \tag{1.6}$$

where $C_t$=$C_s$+$C_b$ [(at.)·m$^{-3}$] is the intra-granular gas concentration (single atoms + bubbles). Eq. (1.6) is formally identical to the equation solved by Booth (1957) for the case of diffusion of single gas atoms in absence of bubbles. With respect to the formulation of Booth, in the formulation of Speight the single atom diffusion coefficient, $D_s$, is replaced by an effective diffusion coefficient

$$D_{eff} = \frac{b}{b+g} D_s . \tag{1.7}$$

Considering the trapping and irradiation-induced resolution effects, the apparent diffusion rate under irradiation is therefore described by a lower (effective) single atom diffusion coefficient, since only a fraction $b/(b+g)$ of the gas – namely, the fraction existing as single atoms – contributes to diffusion, while the remaining fraction $g/(b+g)$ is trapped into immobile bubbles.

Eq. (1.6) is analogous to Eq. (1.2) and solved in the TRANSURANUS code. However, in the current TRANSURANUS model the effective diffusion coefficient, $D_{eff}$, is calculated by means of an empirical correlation (e.g., Eq. (1.3)) instead of applying conversion of $D_s$ by means of Eq. (1.7). Differently, in the present model, Eq. (1.7) is adopted for the calculation of the effective diffusion coefficient. The analytical descriptions, which are used for the parameters $D_s$, $g$, and $b$, are given in the following.

The correlation by Turnbull et al. (1982, 1988) for the single atom diffusion coefficient in $UO_2$, often applied in the fuel performance codes and used by many authors (e.g., (White and Tucker 1983, Bernard et al. 2002, Lösönen 2002)), is adopted in the present work. The correlation describes $D_s$ [m$^2$·s$^{-1}$] as the sum of three terms:

$$D_s = D_1 + D_2 + D_3 , \tag{1.8}$$

where $D_1$ represents high temperature intrinsic diffusion by means of thermally activated vacancies, and $D_2$ and $D_3$ represent the effect of irradiation enhancement. The first two terms are calculated as

$$D_1 = 7.6 \cdot 10^{-10} \, exp\left(-35000 / T\right), \tag{1.9}$$

$$D_2 = 3.22 \cdot 10^{-16} \sqrt{R} \, exp\left(-13800 / T\right), \tag{1.10}$$

where $R$ [W·g$^{-1}$] is the specific power. The purely rating dependent term, $D_3$, is not taken into account here, since it has no visible effect on the diffusion of stable gas atoms (White 1994, Lösönen 2002).

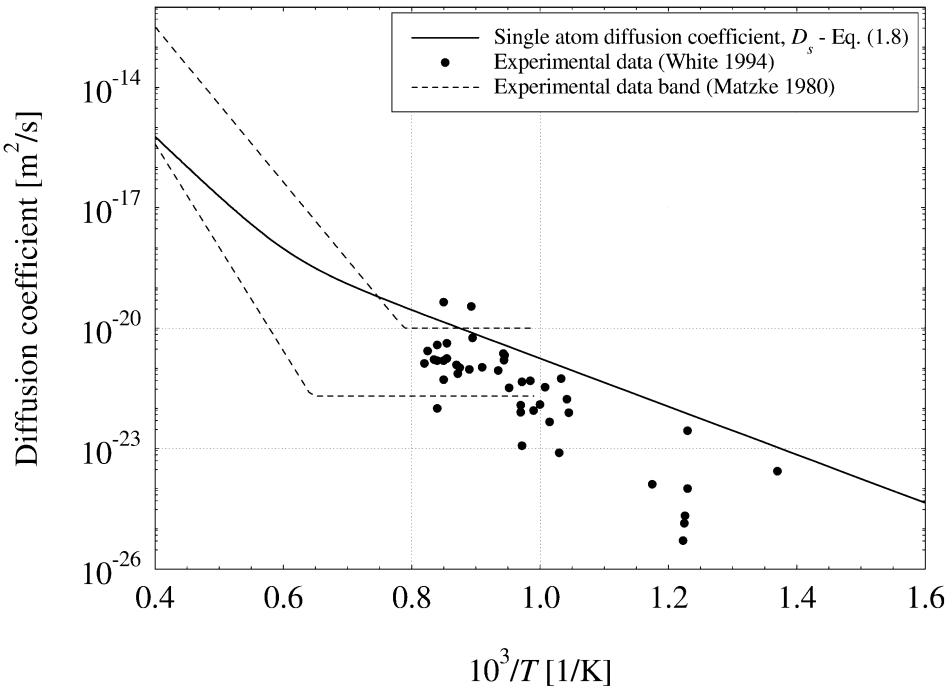


Fig. 1.1. Single atom diffusion coefficient according to Turnbull et al. (1982, 1988) (with $R$=30 W·g$^{-1}$) and experimental data from White (1994) and Matzke (1980).

The resulting single atom diffusion coefficient as a function of the temperature is presented in Fig. 1.1, where experimental data from Matzke (1980) and White (1994) are also shown. It can be noticed that the uncertainties related to the experimental data are extremely high, which unavoidably limits the accuracy achievable in fission gas diffusion calculations. In this respect, the adoption of simple models of fission gas behaviour may be justified.

The trapping and the irradiation-induced resolution parameters (Ham 1958, White and Tucker 1983) are given by

$$g = 4\pi D_s R_b N_b , \tag{1.11}$$

$$b = 3.03 F \pi l_f \left(R_b + Z_0\right)^2 , \tag{1.12}$$

where $N_b$ [(bub.)·m$^{-3}$] is the concentration of bubbles, $R_b$ [m] the mean bubble radius, $F$ [(fiss.)·m$^{-3}$·s$^{-1}$] the fission rate density, $l_f$ [m] the length of a fission fragment track, and $Z_0$ [m] the radius of influence of a fission fragment track. The values $l_f$ =6·10$^{-6}$ m and $Z_0$=10$^{-9}$ m (White and Tucker 1983) are used in the present model, while the calculation of $N_b$ and $R_b$ is performed as described in subsection 1.2.2.

### *1.2.2 Intra-granular fission gas swelling*

Calculating the intra-granular fission gas swelling requires the modelling of the kinetics of the intra-granular bubbles. As resulting from transmission electron microscopy (TEM) examinations of irradiated $UO_2$, the salient characteristics of the intra-granular bubble population are the high concentration (~7·10$^{23}$ (bub.)·m$^{-3}$) and the small, nearly-uniform size of the bubbles (typically < 2 nm

diameter). Bubbles are small enough that the surface-tension stress keeps the gas density near that of solid xenon (Lösönen 2000, Olander and Wongsawaeng 2006). A gas density of ~7 kg·m$^{-3}$, or a gas atomic volume $\Omega$[m$^3$]~3·10$^{-29}$, have been evaluated by Olander and Wongsawaeng (2006) for intra-granular bubbles in irradiated $UO_2$. On this basis, and in consideration of the uncertainties pertaining to the model parameters like the gas atom diffusion coefficient, the present model is founded on the following simplifying assumptions:

(a) The concentration of bubbles remains constant at an initially nucleated level $N_b$=7·10$^{23}$ (bub.)·m$^{-3}$. A decrease of the bubble concentration (from 9·10$^{23}$ to 4.4·10$^{23}$ (bub.)·m$^{-3}$) has been actually observed by Kashibe et al. (1993) when increasing the burn-up of irradiated $UO_2$ from 23 to 83 GWd/t. However, in view of the above mentioned uncertainties, the dependence of the bubble concentration on burn-up is not considered in the model.

(b) A constant value $\Omega$[m$^3$]=3·10$^{-29}$is adopted for the gas atomic volume.

(c) All bubbles are considered to have the same size and the same (spherical) shape.

(d) The intra-granular gas residing in bubbles is equally distributed in the bubbles.

Under the above assumptions, the radius of a bubble containing *m* fission gas atoms is

$$R_b = Bm^{1/3}, \tag{1.13}$$

where $B$[m] = $(3\Omega/4\pi)^{1/3}$ = 2·10$^{-10}$. The number of fission gas atoms contained in each bubble, *m*, is

$$m = C_b / N_b , \tag{1.14}$$

where $C_b$ [(at.)·m$^{-3}$] is the concentration of gas residing in bubbles. Basing on the quasi-stationary approach Eq. (1.5), $C_b$ is estimated as

$$C_b = \left( \frac{g}{g+b} \right)_{t-\Delta t} \cdot C_t , \tag{1.15}$$

where *g* and *b* as calculated at the previous time step ($t$-$\Delta t$) are used.

The fractional volume of intra-granular fission gas swelling, normalized to the unit volume of fuel, is then given by

$$\left( \frac{\Delta V}{V} \right)_{gr} = N_b \left( \frac{4}{3} \pi R_b^3 \right). \tag{1.16}$$

## 1.3 Grain-boundary module

Grain-boundary swelling and FGR are determined by the arrival rate of gas at the grain boundaries. Allowing the rate of transport of fission gas from the fuel grains to the grain boundaries to be calculated, the intra-granular module provides the source term of the grain-boundary module. The latter allows the grain-boundary swelling and the release of fission gas from the grain boundaries to the free volumes in the fuel rod (FGR) to be estimated. The treatment, which is briefly described in subsection 1.3.1, is an extension of the modelling of the kinetics of inter-granular gas pores found in the open literature.

### *1.3.1 Main assumptions*

The main simplifying assumptions, which are used in describing the grain-boundary fission gas behaviour according to the proposed model, are the following:

(I) At $t = 0$, an initial concentration of inter-granular gas pores (nucleation centres), $N_0$ [(por.)·m$^{-2}$], is assumed, and no nucleation of new pores for $t > 0$ is considered. This corresponds to the assumption that the geometric size of the initial population leads to absorption of any newly nucleated pore, giving the effect that the nucleation is a one-off process (White 2004). The choice of $N_0$ is not too critical since the concentration of gas pores falls very quickly once swelling commences (White 2004). In the present model, $N_0$[(por.)·m$^{-2}$] = $4 \cdot 10^{13}$ is adopted, in accordance with (Cheon et al. 2004) and consistently with experimental observations showing values between $1 \cdot 10^{13}$ and $5 \cdot 10^{13}$ (White 2004).

(II) All the fission gas on the grain boundaries is retained in the inter-granular gas pores. This corresponds to the hypothesis of instantaneous absorption of gas atoms at the gas pores since the absorption rate equals the diffusion rate to the boundaries. A more accurate description could be obtained by a solution of the full time-dependent diffusion equation, but numerical solutions indicate this to be an unnecessary refinement (White 2004). This may follow from the fact that the at the grain-boundary gas atom diffusion coefficient, which governs the gas flow from the grain boundary to the inter-granular gas pores, is much higher than the intra-granular gas diffusion coefficient (by a factor of $10^2$-$10^6$ in the temperature range from 1000 to 1700°C (Olander and Van Uffelen 2001)).

(III) The grain-boundary fission gas is equally distributed in the pores.

(IV) All pores have the same size and the same shape (lenticular of circular projection).

(V) The irradiation-induced resolution flux of gas atoms from the inter-granular gas pores to the grain interior is neglected. Although the effect of resolution on inter-granular gas pores is not negligible, a reasonable approximation can be obtained by adopting this assumption (Rest 2003, Spino et al. 2005).

(VI) Once a network of interconnected pores has formed on the grain boundaries, gas can be directly released to the fuel exterior (i.e., the intermediate step of release to the grain edges is not considered).

Given the above assumptions, the kinetics of grain-boundary swelling and FGR may be conveniently considered as resulting from the following effects:

- The growth of inter-granular gas pores through the collection of fission gas atoms and vacancies.
- The mutual interaction between gas pores through coalescence leading to larger but fewer pores.
- The venting of fission gas from the grain boundaries leading to FGR.

The modelling of these effects is discussed below.

### *1.3.2 Growth of gas pores*

Mechanical equilibrium requires that the pressure of the gas in the pore, $p$ [Pa], is balanced by the surface tension force and the hydrostatic stress, $\sigma_h$ [Pa], that is $p = 2\gamma/R_{gp}+\sigma_h$, where $\gamma$ [J·m$^{-2}$] is the $UO_2$/gas specific surface energy, $R_{gp}$ [m] is the radius of curvature of the pore, and $\sigma_h$ is considered to be positive if compressive. $\gamma$ differs from the $UO_2/UO_2$ specific surface energy and this results in lenticular pores with a semi-dihedral angle of approximately 50° (White 2004).

In general, the inter-granular gas pores are over-pressurized and mechanical equilibrium can only be restored by vacancy absorption. The Speight and Beere (1975) model describes the growth (or shrinkage) of the gas pores as proceeding by absorption (or emission) of vacancies generated on the grain boundaries. The vacancy absorption/emission rate at a lenticular pore of circular projection is given by

$$\frac{dn_v}{dt} = \frac{2\pi D_{gb}\delta_{gb}}{kTS}\left(p - \frac{2\gamma}{R_{gp}} - \sigma_h\right). \tag{1.17}$$

where $n_v$ [(vac.)] is the number of vacancies in the pore, $D_{gb}$ [$m^2 \cdot s^{-1}$] is the grain-boundary vacancy diffusion coefficient, $\delta_{gb}$ [m] is the thickness of the diffusion layer in the grain boundary, and $S$ is

$$S = -\left(\left(3 - F_c\right)\cdot\left(1 - F_c\right) + 2\,ln\left(F_c\right)\right)/4, \tag{1.18}$$

where $F_c$ [/] is the fraction of grain boundary covered by gas pores (fractional coverage). In the proposed model, $\delta_{gb}$[m]=$5\cdot10^{-10}$ (Kogai 1997) is adopted along with the expression for the grain-boundary vacancy diffusion coefficient used by Kogai (1997),

$$D_{gb} = 6.9\cdot10^{-4}\,exp\left(-38752/T\right), \tag{1.19}$$

which is a slight modification of that of Reynolds and Burton (1979). The gas pressure in the pore, $p$, for a Van der Waals' gas is given by

$$p = \frac{kT}{\varepsilon\,\Omega_{gb}}, \tag{1.20}$$

where $k$ [J/K] is the Boltzmann constant, $\Omega_{gb}$ [$m^3$] is the atomic (vacancy) volume in the pore, and $\varepsilon$ [/] is the number of vacancies per fission gas atom in the pore. In the proposed model, $\Omega_{gb}$[$m^3$]=$4.09\cdot10^{-29}$ is adopted in line with Kogai (1997).

The pore growth rate can be calculated from the number of gas atoms and vacancies present. The volume, $V_{gp}$ [$m^3$], of a pore comprising $n_g$ fission gas atoms and $n_v$ vacancies is given by

$$V_{gp} = n_g b_{VdW} + n_v\Omega_{gb}, \tag{1.21}$$

where $b$ is the Van der Waals' volume of a fission gas atom. The overall growth rate is therefore determined by the individual rates of change of the fission gas atom and vacancy numbers in the pore. Any addition of fission gas atoms gives rise to a change in the pressure in the pore via Eq. (1.20), which immediately affects the propensity of the cavity to absorb (or emit) vacancies through Eq. (1.17). Also, the hydrostatic stress, $\sigma_h$, acts to inhibit bubble growth through Eq. (1.17).

Given the volume, $V_{gp}$, of a lenticular gas pore of circular projection, its radius of curvature is

$$R_{gp} = \left(\frac{3V_{gp}}{4\pi\varphi(\theta)}\right)^{1/3}, \tag{1.22}$$

where $\theta$ is the semi-dihedral angle of the pore and $\varphi(\theta)$ is the geometric factor relating the volume of a lenticular-shape pore to that of a sphere, calculated as

$$\varphi(\vartheta) = 1 - 1.5\cos\theta + 0.5(\cos\theta)^3. \quad (1.23)$$

In the present model, the conventionally accepted value $\theta$ =50° is adopted.

The projected area of the pore on the grain boundary, $A_{gp}$ [m$^2$], is

$$A_{gp} = \pi(\sin\theta)^2 R_{gp}^2, \quad (1.24)$$

and the fractional coverage, $F_c$ [/], is given by

$$F_c = A_{gp} N_{gp}, \quad (1.25)$$

where $N_{gp}$ is the concentration of inter-granular gas pores. In order to evaluate $S$ through Eq. (1.18), the fractional coverage as calculated at the previous time step is used in the model. The calculation of $N_{gp}$ is dealt with below.

### *1.3.3 Coalescence of gas pores*

In the present model, coalescence is treated as a geometric phenomenon. Growth of inter-granular gas pores leads to mechanical interference and coalescence, and consequent progressive reduction in the concentration of pores. Given that each pore consists of vacancies and gas atoms, the coalescence event must conserve the volume of the interacting pores. In line with White (2004), the treatment of coalescence included in the model is based on the following geometrical reasoning. On the grain boundary, each pore is surrounded by an area of, on average, four times its own projected area, $A_{gp}$, in which no other pore centres can reside. It is easy to demonstrate that this is correct for a uniform population of pores of circular projection. Any pore centre located in this exclusion zone would find its perimeter within the perimeter of the parent pore and coalescence would occur. Any further growth of the projected area of the parent pore by an amount $dA_{gp}$, effectively increases the area of the exclusion zone by $4dA_{gp}$ and opens the possibility that $4N_{gp}\cdot dA_{gp}$ pore centres fall into the exclusion zone. In that event, the pore perimeters interact and coalescence occurs. White assumes that the newly coalesced pore retains the same projected area of the individual parent pores, for which the total rate of loss of pores by coalescence following an increase in area is given by $(\partial N_{gp}/\partial A_{gp}) = -2N^2_{gp}$. Differently, as a result of the assumption that all pores have lenticular shape of circular projection (subsection 1.3.1), the above geometrical reasoning along with the conservation of the total pores volume gives for the present model (see the Appendix for the derivation):

$$\frac{dN_{gp}}{dA_{gp}} = -\frac{6N_{gp}^2}{3 + 4N_{gp}A_{gp}}. \quad (1.26)$$

Eq. (1.26) describes the variation of the pore concentration owing solely to coalescence. Therefore, Eq. (1.26) does not describe the overall variation of the pore concentration at high fractional coverage, $F_c$, when a network of interconnected pores forms leading to FGR, as discussed in subsection 1.3.4.

### *1.3.4 Fission gas release*

It is conventionally assumed that the onset of FGR due to pore interconnection commences after attainment of the saturation value of the fractional coverage $F_c \approx 0.5$ (saturation coverage) (e.g., (Veshchunov 2008)). At this point, it is assumed in the present work that the pore concentration and projected area obey the saturation coverage condition,

$$F_c = N_{gp} A_{gp} = 0.5, \tag{1.27}$$

instead of Eq. (1.26), which implies that a fraction of the gas reaching the grain boundaries is transferred to the fuel exterior to compensate for pore growth. More precisely, in the present simple approach it is assumed that, after attainment of the saturation coverage, any further pore growth is balanced by loss of pores due to FGR in order to satisfy Eq. (1.27). Hence, the evolution of the pore concentration as a function of the pore area is considered as governed by coalescence (subsection 1.3.3) for $F_c < 0.5$ and by FGR after attainment of $F_c$=0.5, and is therefore described by:

$$\begin{aligned} &\frac{dN_{gp}}{dA_{gp}} = -\frac{6N_{gp}^2}{3 + 4N_{gp}A_{gp}} && \text{if } N_{gp}A_{gp} < 0.5 \\ &\frac{dN_{gp}}{dA_{gp}} = -\frac{N_{gp}}{A_{gp}} && \textit{if } N_{gp}A_{gp} = 0.5. \end{aligned} \tag{1.28}$$

Eq. (1.28) is used within the model to evaluate the observed reduction of the concentration of inter-granular gas pores in $UO_2$ throughout irradiation (White 2004). In Fig. 1.2, Eq (1.28) is compared with the experimental data of pore concentrations and corresponding mean pore projected areas from White et al. (2006). The bifurcation between the dashed line (Eq. (1.26)) and the full line (Eq. (1.28)) corresponds to the attainment of the saturation coverage. In view of the adopted simplifications and involved uncertainties, Eq. (1.28) appears to reasonably conform to the data.

According to the above discussed approach, and considering that each pore contains $n_g$ fission gas atoms (subsection 1.3.2), the FGR rate is given by

$$\begin{aligned} &\frac{dn_{fgr}}{dt} = 0 && \textit{if } N_{gp}A_{gp} < 0.5 \\ &\frac{dn_{fgr}}{dt} = n_g \frac{N_{gp}}{A_{gp}} \frac{dA_{gp}}{dt} && \textit{if } N_{gp}A_{gp} = 0.5. \end{aligned} \tag{1.29}$$

where $n_{fgr}$ is the number of gas atoms released into the fuel rod free volumes. This simple treatment allows to describe the incubation behaviour of FGR as well as its dependence on the hydrostatic stress in the fuel (through Eq. (1.17)) and coupling with the swelling, on a physical basis.

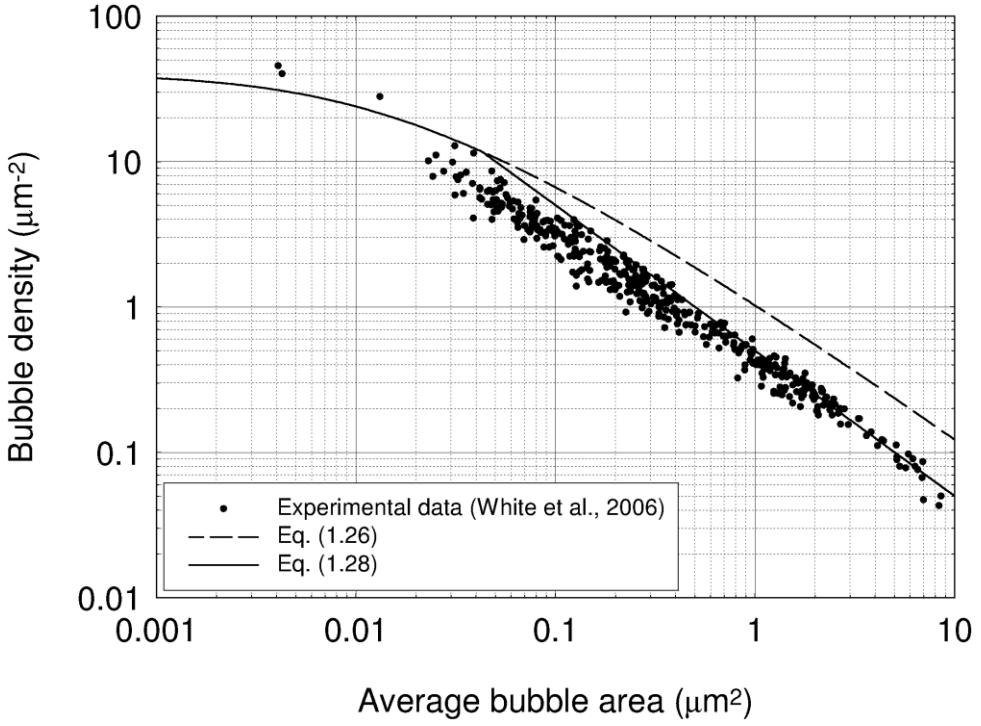


Fig. 1.2. Variation of the pore concentration with the mean bubble projected area. Experimental data from White et al. (2006) (see subsection 1.4) are compared with the present model Eq. (1.28). Eq. (1.26) is also shown. An initial pore concentration $N_0 = 4 \cdot 10^{13}$ (por.)·m$^{-2}$ is considered.

### *1.3.5 Grain-boundary swelling*

The equations presented so far allow to calculate the time evolution of the concentration and the size of the inter-granular gas pores. Since a uniform population of pores is considered (subsection 1.3.1), the fractional volume of grain-boundary fission gas swelling, normalized to the unit volume of fuel, is calculated as

$$\left(\frac{\Delta V}{V}\right)_{gb} = \frac{1}{2}\frac{N_{gp}}{(1/3)\,r_{gr}}\left(\frac{4}{3}\pi\, R_{gp}^3\, \varphi(\theta)\right). \tag{1.30}$$

where $r_{gr}$ [m] is the radius of the spherical grains, and the factor 1/2 is introduced because an inter-granular gas pore is shared by two neighboring grains.

### *1.3.6 Calculational sequence*

The following calculational sequence is adopted in applying the grain-boundary module at each computational time step:

(i) The rate of increase of the number of gas atoms per inter-granular gas pore, $n_g$, is calculated from the arrival rate of gas at the grain boundaries provided by the intra-granular module, and considering the gas as uniformly distributed in the pores (subsection 1.3.1).

(ii) The pore growth rate is calculated on the basis of the Speight and Beere (1975) equation (subsection 1.3.2), giving the time evolution of the temperature- and hydrostatic stress-dependent pore size.

(iii) The decrease of pore concentration through coalescence/FGR, as well as the FGR rate, are calculated by means of Eq. (1.28) using the newly projected area after the effect of pore growth.

(iv) The grain-boundary fission gas swelling is calculated by means of Eq. (1.30).

## 1.4 Stand-alone model verification

The stand-alone model of fission gas swelling and release, which incorporates the features described in subsections 1.2 and 1.3, has been applied to the analysis of the cases of the AGR/Halden Ramp Test Programme (White et al. 2006). This has allowed a first verification of the model through a systematic comparison with the available experimental data of local grain-boundary fission gas swelling, as discussed in subsection 1.4.1.

### *1.4.1 Fission gas swelling database*

The AGR/Halden Ramp Test Programme (White et al. 2006) involved the base-irradiation and subsequent ramp test of Advanced Gas cooled Reactor (AGR) $UO_2$ fuel rods in the Halden Reactor using fuels that were base-irradiated in the Hinkley Point, Torness and Halden Reactors up to burn-ups of around 21 GWd/tU. Extensive transmission electron microscopy (TEM) and scanning electron microscopy (SEM) examinations of the fuel from all the experiments were performed to study the intra-granular and grain-boundary fission gas swelling, respectively. The results of the study have been made available through the IFPE database (Sartori et al. 2010). Some details of the different irradiation tests and SEM examinations, on which the experimental data of grain-boundary swelling considered in the present work are referred to, are given in Table 1.1. The fuel rods were subjected to either ramps – designated fast or slow – or power cycling. The schematic form of the ramp is shown in Fig. 1.3 and the times and powers of each stage are summarised in Table 1.2. Note that the slow ramps are those in which $\tau_{2a}$ is of the order of 45 min and the fast ramps are those for which $\tau_{2a}$ is from 1–2 min. The two power-cycled fuel rods were subjected to 115 four-hour cycles, the details of which are

Table 1.1.
Details of irradiation tests and PIE/SEM of the AGR/Halden Ramp Test Programme.

| Rod identifier | Burn-up [GWd/tU] | Ramp type | Peak rating [kW/m] | Hold-time | SEM zones | Boundaries measured |
|---|---|---|---|---|---|---|
| 4000 | 20.7 | Fast | 40 | 30.0 min | 5 | 48 |
| 4004 | 20.5 | Fast | 40 | 2.38 min | 6 | 44 |
| 4005 | 20.8 | Fast | 40 | 2.0 min | 5 | 39 |
| 4064 | 20.1 | Slow | 43 | – | 5 | 63 |
| 4065 | 9.3 | Slow | 41.8 | – | 5 | 43 |
| 4159 | 20.2 | Cycles | 18-26 | 115·4 h | 5 | 56 |
| 4160 | 20.1 | Cycled | 18-26 | 115·4 h | 6 | 45 |
| 4162 | 12.6 | Slow | 40 | – | 4 | 47 |
| 4163 | 12.6 | Fast | 40 | 2.0 min | 5 | 37 |
| | | | | | 46 | 422 |

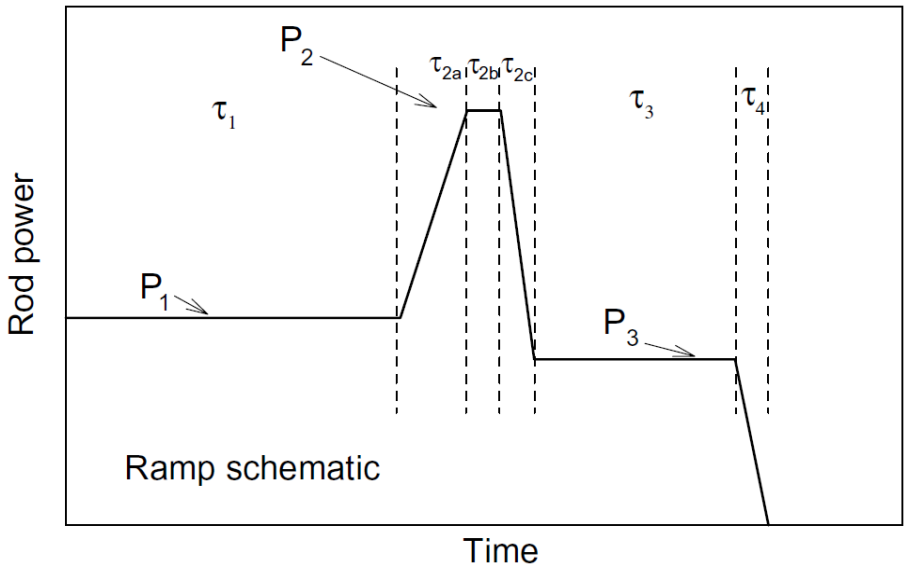


Fig. 1.3. Schematic of the terminal ramp in the irradiation tests of the AGR/Halden Ramp Test Programme (White et al. 2006).

summarised in Table 1.3. The rods were encased in a Zircaloy shroud for irradiation in the Halden Reactor and the interspace was pre-filled (usually) with helium although a mixture of helium and argon was employed in one of the power-cycled rods, which resulted in higher cladding temperatures and consequently higher fuel temperatures.

For each test, the SEM examinations have been performed at different zones of the fuel specimen, allowing the construction of a wide database of grain boundary swelling measurements. Moreover,

Table 1.2
Details of power ramps – fast and slow ramps.

| Rod identifier | Power 1 [kW/m] | $\tau_1$ | $\tau_{2a}$ [min] | Power 2 [kW/m] | $\tau_{2b}$ [min] | $\tau_{2c}$ [s] | Power 3 [kW/m] | $\tau_3$ [min] | $\tau_4$ |
|---|---|---|---|---|---|---|---|---|---|
| 4000 | 14.0 | 12d | 1.52 | 40.0 | 30.0 | 100 | 14.0 | 99.0 | SCRAM |
| 4004 | 14.0 | 12d | 1.97 | 40.0 | 2.38 | 90 | 14.0 | 99.0 | SCRAM |
| 4005 | 14.0 | 12d | 1.32 | 40.0 | 2.0 | – | SCRAM | – | – |
| 4064 | 20.0 | 15wk | 47.0 | 43.0 | 0.0 | – | SCRAM | – | – |
| 4065 | 19.3 | 3wk | 47.0 | 41.8 | 0.0 | – | SCRAM | – | – |
| 4162 | 18.0 | 3wk | 45.0 | 40 | 0.0 | 40 | 18.0 | 6 | – |
| 4163 | 18.0 | 3wk | 2.0 | 40.0 | 2.0 | 80 | SCRAM | – | – |

Table 1.3
Details of power ramps – power-cycling cases.

| Rod identifier | Power 1 [kW/m] | Time 1 | Ramp up | Power up [kW/m] | Ramp down | Power down [kW/m] | Deconditioning [kW/m] | Last phase |
|---|---|---|---|---|---|---|---|---|
| 4159 and 4160 | 18.0 | 7d | 30 min | 26.0 for 1h | 30 min | 18.0 for 2h | 18.0 for 2d | Shut-down |
| | | | 115 – 4h cycles | | | | | |

the specific power, temperature, and hydrostatic stress of each SEM zone were calculated by means of the ENIGMA fuel performance code (White et al. 2006), thus providing the basis for reconstruction of the experiments and verification of fission gas swelling models. In Table 1.4, a summary of the experimental data of grain-boundary swelling, $(\Delta V/V)_{gb,\ exp}$, for each SEM zone is given. All the grain-boundary swelling data provided through the Programme are reported, except that related to the SEM zone 4160-G, which has been not used in the present work (see subsection 1.4.2).

### *1.4.2 Model calculations*

The stand-alone model simulations of the ramp tests performed within the AGR/Halden Ramp Test Programme have been carried out coherently with the fuel fabrication data and the details of the irradiation histories provided in (White et al. 2006). Moreover, in view of the lack of information on the base-irradiation details, the following hypotheses have been made in order to assess the initial conditions for the analysis of the ramp tests:

- All the fission gas generated during the base-irradiation is considered to be retained inside the fuel grains at the beginning of the ramp tests. This assumption is consistent with the observation that, in all of the cases studied, the base-irradiation resulted in negligible fission gas release and microstructural changes (White et al. 2006).
- The fuel grain size is assumed to remain constant throughout the ramp tests, and equal to the measured value at the end of each test. Since some grain growth is expected to occur during the ramp tests, this assumption may result in some under-estimation of the arrival rate of gas at the grain boundaries as a consequence of the over-estimation of the grain size during the early stages of the ramp tests.

Table 1.4.
Summary of experimental data of grain-boundary swelling.

| SEM zone | $(\Delta V/V)_{gb}$ [%] | SEM zone | $(\Delta V/V)_{gb}$ [%] | SEM zone | $(\Delta V/V)_{gb}$ [%] |
|---|---|---|---|---|---|
| 4000-A | 0.97±0.35 | 4064-A | 1.07±0.58 | 4160-A | 2.61±0.57 |
| 4000-B | 0.68±0.12 | 4064-B | 0.86±0.32 | 4160-B | 2.30±0.56 |
| 4000-C | 0.53±0.10 | 4064-C | 0.63±0.22 | 4160-C | 2.60±0.36 |
| 4000-D | 0.46±0.10 | 4064-D | 0.74±0.19 | 4160-D | 1.64±0.20 |
| 4000-F | 0.17±0.4 | 4064-E | 0.59±0.26 | 4160-E | 1.22±0.21 |
| | | | | 4160-F | 0.74±0.09 |
| 4004-A | 0.62±0.13 | 4065-A | 1.25±0.43 | 4162-A | 0.70±0.26 |
| 4004-B | 0.70±0.26 | 4065-B | 1.35±0.30 | 4162-B | 0.46±0.17 |
| 4004-C | 0.44±0.11 | 4065-C | 0.97±0.26 | 4162-C | 0.43±0.18 |
| 4004-D | 0.56±0.15 | 4065-D | 0.79±0.15 | 4162-D | 0.43±0.22 |
| 4004-E | 0.27±0.07 | 4065-E | 0.21 | | |
| 4004-F | 0.16 | | | | |
| 4005-A | 0.94±0.16 | 4159-A | 1.85±0.22 | 4163-A | 0.60±0.20 |
| 4005-B | 0.57±0.20 | 4159-B | 1.67±0.26 | 4163-B | 0.59±0.18 |
| 4005-C | 0.42±0.12 | 4159-C | 1.37±0.16 | 4163-C | 0.35±0.10 |
| 4005-D | 0.54±0.15 | 4159-D | 1.06±0.15 | 4163-D | 0.40±0.06 |
| 4005-E | 0.27±0.02 | 4159-E | 0.91±0.28 | 4163-E | 0.26±0.13 |

The results of the calculations are presented in Fig. 1.4. The comparison between the values of grain boundary swelling calculated by the model and the experimental data points out a reasonable overall agreement. An average under-estimation is observed, which may be in some degree ascribed to under-estimation of the arrival rate of gas at the grain boundaries as a consequence of the hypothesis of constant grain size, as discussed above. Considering the uncertainty associated with the measurements (Table 1.4), the predicted values deviate on average from the experimental ones by a factor of about 1.7, which appears to be consistent with the involved uncertainties and satisfactory in view of the application of the model to integral fuel rod calculations.

In conclusion, the stand-alone model calculations allowed a first assessment of the prediction capability of the proposed model against experimental data of grain boundary swelling, which pointed out a satisfactory agreement without any fitting of model parameters. Indeed, the implementation of the model in the TRANSURANUS code allowed to extend its verification base through comparison of the calculations with integral experimental data of FGR, as discussed in the next section.

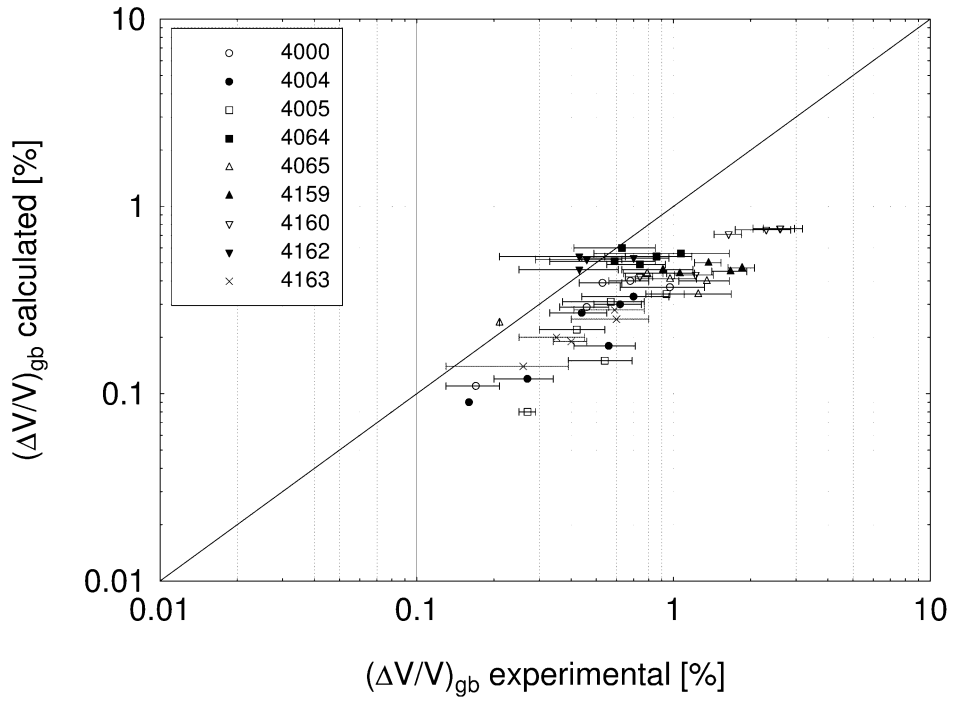


Fig. 1.4. Predicted values of grain-boundary swelling compared with the experimental data from the AGR/Halden Ramp Test Programme.

## 2. MODEL APPLICATION IN THE FUMEX-III PROJECT

### 2.1 Introduction

A first implementation in the TRANSURANUS code of the model of fission gas swelling and release described in section 1 has been very recently achieved. The implementation has been carried out by incorporating the model in the mathematical-numerical structure of the code, providing a consistent matching between the stress-dependent swelling and FGR calculations and the thermo-mechanical analysis.

The modified version of the TRANSURANUS code, which adopts the new fission gas swelling and release model, has been applied to the analysis of LWR-$UO_2$ fuel rods, including a number of priority cases of FUMEX-III. These analyses have allowed to preliminarily assess the prediction capability of the modified TRANSURANUS version in terms of FGR predictions, through comparison with the available experimental data.

Table 2.1 lists the priority cases of the Fumex-III Project, which are all included in the IFPE database (Sartori et al. 2010). In the present work, the cases of the Super-Ramp and Inter-Ramp Projects, including those comprised in the FUMEX-III Project, have been analyzed. The results in terms of FGR predictions are presented in subsection 2.2.

Table 2.1.
Matrix of priority cases in the FUMEX-III project. Cases in italics are considered in the present work.

| Plant type | MOX | Mechanical interaction | | Severe transients | | FGR, Temperature | | | |
|---|---|---|---|---|---|---|---|---|---|
| | | PCMI | PCI | LOCA | RIA | Load follow transients | Transients | Gd/Nb | Normal operation FGR |
| LWR | IFA629<br><br>PRIMO -BD8 | RISØ3 -GE7<br>OSIRIS -H09 | *INTER-RAMP*<br>- *BR 1, DR 1*<br>- *HR 2-5*<br>- *HS 1-2*, HS 3<br>- *LR 1*, LR 2-5<br>- LS 1,4, *LS 2-3*<br>- *TR 1*, TS 1<br>*SUPER-RAMP*<br>- *PW3*<br>- *PK6* | IFA 650.2 | FK1<br>FK2 | IFA 519.8/9 -DC -DK | IFA535 5 - rod 809<br>Risø3 - II5 | GAIN Gd - 301 - 701 | US 16x16 (PWR) -TSQ002 -TSQ022<br>AREVA (idealized) |
| WWER | | | | | | | MIR Ramp - rod 41 - rod 48 - rod 50 - rod 51 | | US 16x16 (PWR) - TSQ022 (ann. fuel)<br>GINNA - solid fuel - ann. fuel |
| CANDU | CNEA - A1.2 - A1.3 - A1.4 - A3 - A4 | RISØ2 -GE-m<br>RISØ3 -II3 (low bu) | | FIO 131 | | | IRDMR - FIO 118 - FIO 119 (7 rods) | | PITESTI - RO51 - RO89<br>AECL NRU |

## 2.2 Simulation of the Super-Ramp and Inter-Ramp cases

### *2.2.1 Experimental databases*

The datasets of the Super-Ramp and Inter-Ramp Projects (Djurle 1979, Djurle 1984) refer to PWR-$UO_2$ and BWR-$UO_2$ fuel rods, respectively, subjected to power ramps in the Studsvik reactor R2 after base-irradiation. The Super-Ramp rods were irradiated in a burn-up range comprised between 28 and 45 MWd/kgU, while those of Inter-Ramp experienced burn-ups of 8-20 MWd/kgU. The main features of the different groups of rods are summarized in Tables 2.2 and 2.3. An example of base irradiation and power ramp is shown in Fig. 2.1, which refers to the Super-Ramp PK1-2 rod. During the ramp tests, the Super-Ramp rods were raised from a conditioning power of around 25 kW/m to a ramp terminal level of 41-51 kW/m, with a ramp rate of 8-11 kW/(m·min) and a holding time of 12 h (or 1 min, for the PK2-4 rod). The Inter-Ramp rods were raised from a conditioning power of 23-32 kW/m to a ramp terminal level of 38-51 kW/m, with a ramp rate of 4-5 kW/(m·min) and a holding time of 24 h (or 26 min, for the HS1 rod). The calculations described in this report have been carried out coherently with the power histories and coolant conditions from beginning-of-life to the end of ramp test, using the manufacturing specifications and pre-irradiation characterization data of the analyzed rods (Djurle 1979, Djurle 1984). Experimental data of FGR are available for 18 cases of Super-Ramp and 11 cases of Inter-Ramp. All these cases are considered in the following, except for one Super-Ramp case (PK4-S) because the corresponding experimental FGR is stated as unreliable (Djurle 1984).

Table 2.2.
Main features of the PWR Super-Ramp rods.

| Group | Diametral gap size [μm] | $UO_2$ density [%TD] | Average burn-up [GWd/tU] | Enrichment [wt% $^{235}U$] | Average grain size [μm] |
|---|---|---|---|---|---|
| PK1 | 191–200 | 95* | 33–36 | 3.20 | 6.0 |
| PK2 | 145 | 94* | 41–45 | 3.21 | 5.5 |
| PK4 | 167–169 | 94* | 33–34 | 3.19 | 5.5 |
| PK6 | 145–146 | 95* | 34–37 | 2.99 | 22.0 |
| PW3 | 170 | 94** | 28–31 | 8.26 | 10.5 |
| PW5 | 162–165 | 95** | 32–33 | 5.74 | 16.9 |

*Calculated from pellet density measurements. **Calculated from measurements of pellet weights and dimensions.

Table 2.3.
Main features of the BWR Inter-Ramp rods.

| Group | Diametral gap size [μm] | $UO_2$ density° [%TD] | Average burn-up [GWd/tU] | Enrichment [wt% $^{235}U$] | Average grain size [μm] |
|---|---|---|---|---|---|
| BR | 250 | 95 | 19.9 | 3.50 | 8.4 |
| DR | 150 | 93 | 7.9 | 2.82 | 10.9 |
| HR | 150 | 95 | 16.6–19.8 | 3.50 | 8.4 |
| HS | 150 | 95 | 16.6–19.3 | 3.50 | 8.4 |
| LR | 150 | 95 | 8.5–10.3 | 2.82 | 8.3 |
| LS | 150 | 95 | 8.2–10.4 | 2.82 | 8.3 |
| TR | 80 | 95 | 10 | 2.82 | 8.3 |
| TS | 80 | 95 | 9.8 | 2.82 | 8.3 |

°Design specifications.

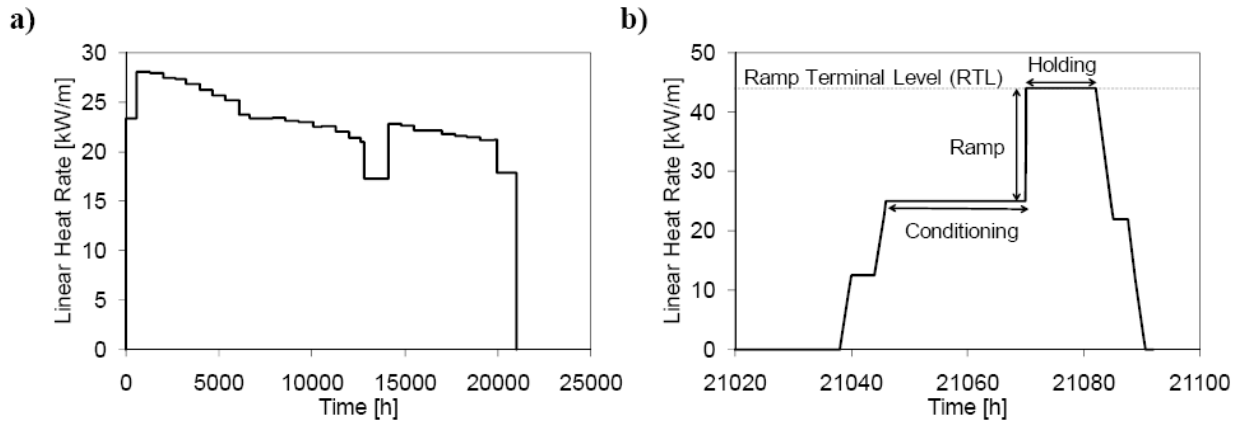


Fig. 2.1. Input power history in axial peak position during a) base irradiation and b) power ramp for the Super-Ramp PK1-2 rod.

### *2.2.2 Results*

The experimental data of FGR have been compared with the results obtained using the modified version of the TRANSURANUS code, which includes the fission gas swelling and release model described in section 1. The comparison between the calculated and the experimental FGR at the end of the ramp tests for the Super-Ramp cases is presented in Fig. 2.2. The overall agreement is good. The predicted values deviate on average from the experimental ones by a factor of about 1.5, which is satisfactory in view of the maximum deviation (factor of 2) commonly regarded as acceptable for FGR predictions.

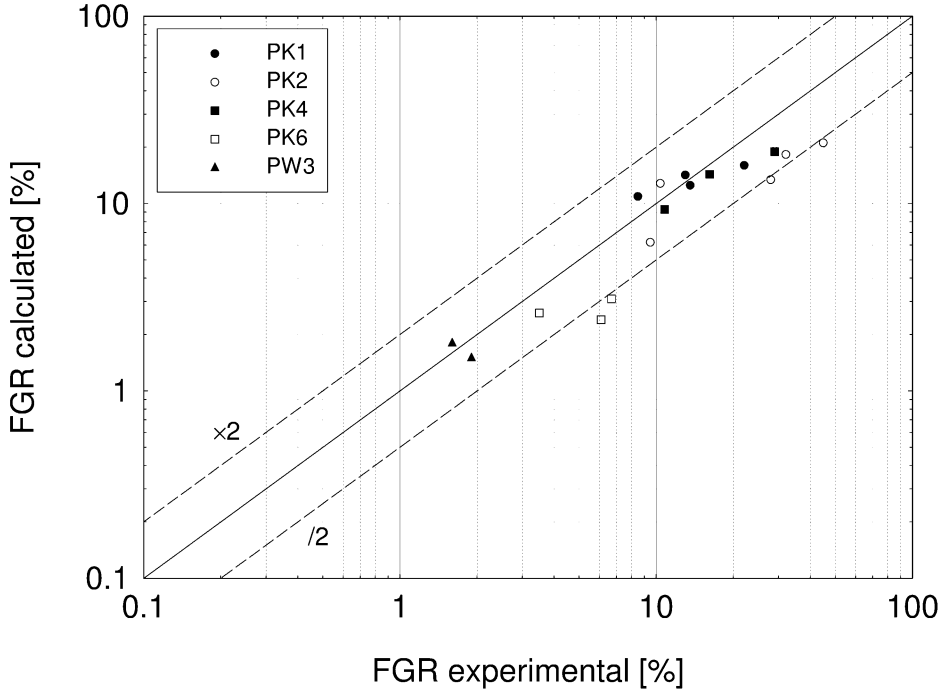


Fig. 2.2. Predicted values of FGR compared with the experimental data for the Super-Ramp tests. The cases belonging to the groups PK6 and PW3 are included in the FUMEX-III Project.

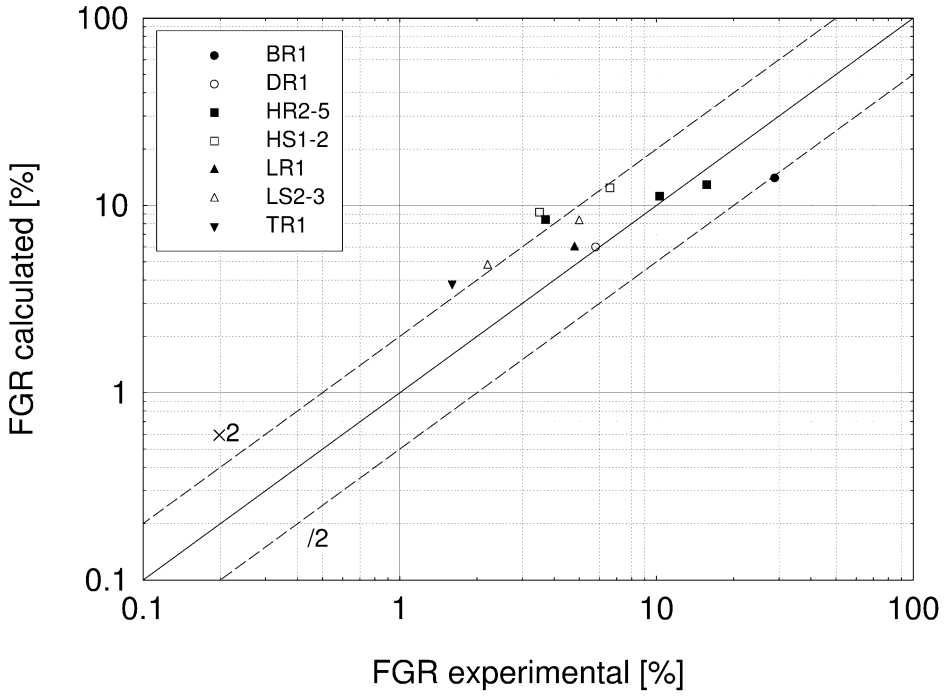


Fig. 2.3. Predicted values of FGR compared with the experimental data for the Inter-Ramp tests. All the cases are included in the FUMEX-III Project.

The comparison between the calculated and the experimental FGR at the end of the ramp tests for the Inter-Ramp cases is presented in Fig. 2.3. The average deviation between predicted and experimental values is of a factor of about 1.8, which again may be regarded as satisfactory as it lies within the acceptability band of a factor of 2. However, differently from the Super-Ramp cases, a significant over-prediction is observed in many cases, which requires further investigation.

The results of the analyses of the Super-Ramp and Inter-Ramp cases are comprehensively summarized in Fig. 2.4, where the predictions of the modified TRANSURANUS version are compared with those obtained using the current TRANSURANUS version. In particular, the standard FGR model of TRANSURANUS and the *ITU model* have been adopted (see subsection 1.1.2). When considering all the cases of the Super-Ramp and Inter-Ramp datasets, the average deviation between predicted and experimental values obtained with the modified TRANSURANUS version (present work) is of a factor of about 1.6. On the other hand, an average deviation of a factor of about 2.1 is associated with the use of the current version of TRANSURANUS with the standard model. These results point out that the new model may allow a significant improvement of the FGR predictions in the simulation of power ramps. When using the current version of TRANSURANUS with the *ITU model*, which is a specific treatment of power ramps, an average deviation of a factor of about 1.6 is obtained, very close to that associated with the modified TRANSURANUS version. The presence of a number of cases, where the predictions of the *ITU model* are more accurate, suggests that taking into account the burst release effect due to pellet micro-cracking during rapid power changes represents an advisable development of the new model.

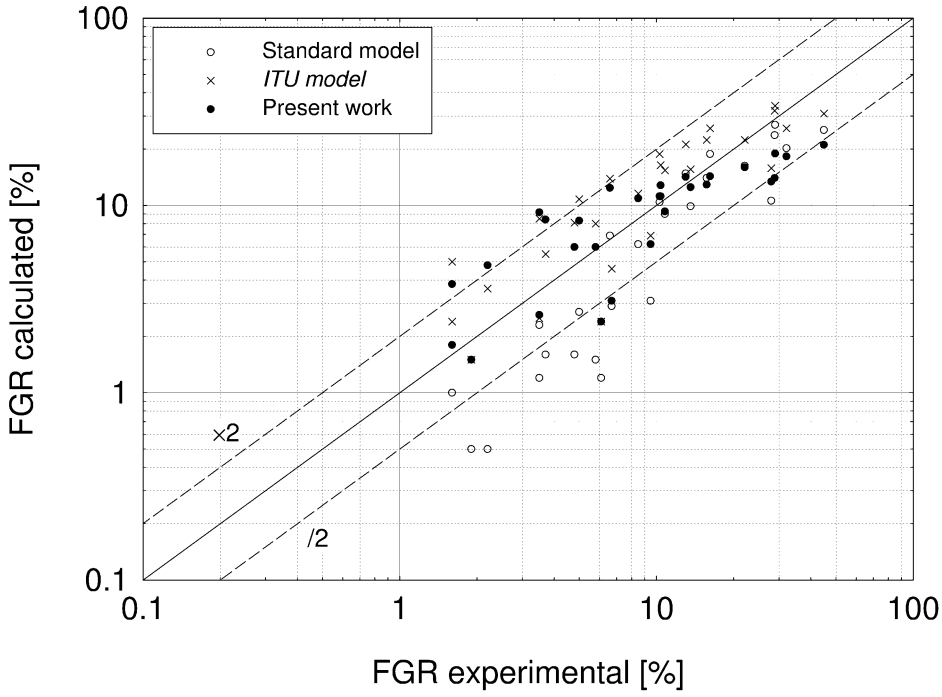


Fig. 2.4. Predicted values of FGR compared with the experimental data for the Super-Ramp and Inter-Ramp tests. Comparison is given between the TRANSURANUS results obtained by using different FGR models.

## CONCLUSIONS AND PERSPECTIVES

In view of the specific research objectives of FUMEX-III, a new model of fission gas swelling and release in irradiated $UO_2$ fuel has been recently developed for the TRANSURANUS code, in the frame of a collaboration between the POLIMI and the ITU. The model calculates the fission gas swelling and release as inherently coupled phenomena, through a description of the underlying microscopic processes. In particular, the connection between the diffusion of fission gas and the kinetics of intra-granular bubbles is considered, and the growth, coalescence, and interlinkage of inter-granular gas pores is modelled along with their dependence on the hydrostatic stress to provide a physics-based treatment of the fission gas swelling and release. The model is as simple as is consistent with the uncertainties pertaining to the parameters and reasonable computational costs.

The prediction capability of the stand-alone model has been assessed through the analysis of the cases of the AGR/Halden Ramp Test Programme, which comprises base-irradiation and ramp tests of AGR-$UO_2$ fuel rods. The systematic comparison of the calculation results with the experimental data of grain-boundary fission gas swelling pointed out a satisfactory agreement, indicating that the model is fit for use within the TRANSURANUS code.

A first implementation of the new model in the TRANSURANUS code has been carried out, and integral analyses of LWR-$UO_2$ fuel rods have been performed. In particular, the modified code version incorporating the new model has been applied to the simulation of the power ramp-tested PWR/BWR fuel rods of the Super-Ramp and Inter-Ramp Projects, including the priority cases of FUMEX-III. These analyses have allowed to assess the prediction capability of the modified TRANSURANUS version in terms of fission gas release predictions, through comparison with the available experimental data. Even if preliminary, the results are promising and indicate that the new physics-based model may allow to satisfactorily analyze the FGR under both normal and transient reactor conditions.

Further development is of interest in perspective as concerns several modelling aspects. In particular, the burst release effect due to pellet micro-cracking during fast power changes is presently not considered in the model, while taking into account this contribution may allow a more proper representation of the fuel behaviour under transient reactor conditions. Also, a suitable treatment of the athermal release processes is to be introduced for a complete physical description of the fission gas release. Moreover, the development of a specific treatment of the swelling and fission gas release contributions resulting from the high burn-up structure formation is needed in view of the adequate analysis of high burn-up fuel. Finally, given the physical basis of the model, the extension of its range of application to different fuel types (e.g., MOX) is envisaged.

(This page has been intentionally left blank)

## REFERENCES


Aybar H.S., Ortego P. (2005). A Review of Nuclear Fuel Performance Codes, Progress in Nuclear Energy, Vol. 46, No 2, pp. 127-141.

Bernard L.C., Jacoud J.L., Vesco P. (2002). An efficient model for the analysis of fission gas release, Journal of Nuclear Materials, Vol. 302, pp. 125-134.

Booth A.H. (1957). A Method of Calculating Gas Diffusion from $UO_2$ Fuel and its Application to the X-2-f Loop Test, AECL-496, Atomic Energy of Canada Ltd.

Cacuci (2010). Handbook of Nuclear Engineering, Dan Gabriel Cacuci (Ed.), Volume 3, Chapter 13.

Chantoin P., Turnbull J.A., Wiesenack W. (1997). How Good is Fuel Modelling at Extended Burn-up?, Nuclear Engineering International, Vol. 42, No. 518, pp. 32-36.

Cheon J-S., Koo Y.-H., Lee B-H., Oh J-Y., Sohn D.-S. (2004). Modeling of a Pellet-Clad Mechanical Interaction in LWR Fuel by Considering Gaseous Swelling, Proceedings of the Seminar on Pellet-clad Interaction in Water Reactor Fuels, Aix-en-Provence, France, March 9-11, 2004, pp. 191-202.

Djurle S. (1979). The Studsvik Inter-Ramp Project, Final Report STUDSVIK-STIR-53, Studsvik AB Atomenergi, Sweden.

Djurle S. (1984). The Super-Ramp Project, Final Report STUDSVIK-STSR-32, Studsvik Energiteknik AB, Nykoping, Sweden.

Ham F.S. (1958). Theory of diffusion-limited precipitation, Journal of Physics and Chemistry of Solids, Vol. 6, pp. 335-351.

IAEA (2011). Fuel Modelling at extended burnup (Fumex-II), Report of a coordinated research project, IAEA TECDOC (in press).

Killeen J., Turnbull J.A., Sartori E. (2007). Fuel Modelling at Extended Burnup: IAEA Coordinated Research Project FUMEX-II, Proceedings of International LWR Fuel Performance Meeting, American Nuclear Society, San Francisco, California, USA, September 30-October 3, 2007, p. 261.

Kashibe S., Une K. (1997). Effect of external restraint on bubble swelling in $UO_2$ fuels, Journal of Nuclear Materials, Vol. 247, pp. 138-146.

Kashibe S., Une K., Nogita K. (1993). Formation and growth of intragranular fission gas bubbles in $UO_2$ fuels with burnup of 6-83 GWd/t, Journal of Nuclear Materials, Vol. 206, pp. 22-34.

Killeen J., Sartori E., McGrath M. (2009). FUMEX-III: A New IAEA Coordinated Research Project on Fuel Modelling at Extended Burnup, Proceedings of the International Conference on Water Reactor Fuel Performance (WRFPM - Top Fuel 2009), Paris, France, September 6-10, 2009, pp. 336-343.

Koo Y.-H., Lee B.-H., Sohn D.-S. (1999). COSMOS: a computer code to analyze LWR $UO_2$ and MOX fuel up to high burnup, Annals of Nuclear Energy, Vol. 26, pp. 47-67.

Lassmann K (1992). TRANSURANUS: a fuel rod analysis code ready for use, Journal of Nuclear Materials, Vol. 188, pp. 295-302.

Lassmann K (2001). The TRANSURANUS Code – Past, Present and Future (Review Article), ITU Activity Report 2001 - EUR 20252, ISBN 92-894-3639-5, p. 16.

Lassmann K., Benk H. (2000). Numerical algorithms for intragranular fission gas release, Journal of Nuclear Materials, Vol. 280, pp. 127-135.

Lassmann K., Schubert A., Van Uffelen P., Győri C., van de Laar J. (2011). TRANSURANUS Handbook, Copyright ©1975-2011, Institute for Transuranium Elements, Karlsruhe, Germany.

Lösönen P. (2000). On the behaviour of intragranular fission gas in $UO_2$ fuel, Journal of Nuclear Materials, Vol. 280, pp. 56-72.

Lösönen P. (2002). Modelling intragranular fission gas release in irradiation of sintered LWR $UO_2$ fuel, Journal of Nuclear Materials, Vol. 304, pp. 29-49.

Luzzi L. (2008). Presentation given at the 1st Research Coordination Meeting of FUMEX-III, Vienna, Austria, December 10-12, 2008.

MATPRO (1979). MATPRO-Version 11 – A Handbook of Material Properties for Use in the Analysis of LWR Fuel Rod Behaviour, NUREG/CR-0497, TREE-1280.

Matzke H. (1980). Gas release mechanisms in $UO_2$ – a critical review, Radiation Effects, Vol. 53, p. 219-242.

Misfeldt I. (1983). The D-COM Blind Problem on Fission Gas Release: Experimental Description and Results, Summary report on OECD-NEA-CSNI/IAEA Specialists' Meeting on Water Reactor Fuel Safety and Fission Product Release in Off-Normal and Accident Conditions", IAEA-IWGFPT/16, pp. 411-422.

Mogensen M., Walker C.T., Ray I.L.F., Coquerelle M. (1985). Journal of Nuclear Materials, Vol. 131, pp. 162-171.

Sartori E., Killeen J., Turnbull J.A. (2010). International Fuel Performance Experiments (IFPE) Database, OECD-NEA, http://www.nea.fr/html/science/fuel/ifpelst.html.

Olander D.R. (1976). Fundamental aspects of nuclear reactor fuel elements, Technical Information Center - Energy Research and Development Administration, University of California, Berkeley.

Olander D.R., Van Uffelen P. (2001). On the role of grain boundary diffusion in fission gas release, Journal of Nuclear Materials, Vol. 288, pp. 137-147.

Olander D.R., Wongsawaeng D. (2006). Re-solution of fission gas – A review: Part I. Intragranular bubbles. Journal of Nuclear Materials, Vol. 354, pp. 94-109.

Pastore G., Botazzoli P., Di Marcello V., Luzzi L. (2009a). Simulation of Power Ramp Tested LWR Fuel Rods by means of the TRANSURANUS Code, Proceedings of the International Conference on Water Reactor Fuel Performance (WRFPM - Top Fuel 2009), Paris, France, September 6-10, 2009, pp. 223-232.

Pastore G., Botazzoli P., Di Marcello V., Luzzi L. (2009b). Assessment of the Prediction Capability of the TRANSURANUS Fuel Performance Code on the Basis of Power Ramp Tested LWR Fuel Rods, Proceedings of the 8th International Conference on WWER Fuel Performance, Modelling and Experimental Support, Bourgas, Bulgaria, September 26-October 4, 2009, pp. 300-308.

Rest J. (2003). The effect of irradiation-induced gas-atom re-solution on grain-boundary bubble growth, Journal of Nuclear Materials, Vol. 321, pp. 305-312.

Reynolds G.L., Burton B. (1979). Grain-boundary diffusion in uranium dioxide: The correlation between sintering and creep and a reinterpretation of creep mechanism, Journal of Nuclear Materials, Vol. 82, pp. 22-25.

Speight M.V. (1969). A Calculation on the Migration of Fission Gas in Material Exhibiting Precipitation and Re-solution of Gas Atoms Under Irradiation, Nuclear Science and Engineering, Vol. 37, pp. 180-185.

Speight M.V., Beere W. (1975). Vacancy Potential and Void Growth on Grain Boundaries, Metal Science, Vol. 9, pp. 190-191.

Spino J., Rest J., Goll W., Walker C.T. (2005). Matrix swelling rate and cavity volume balance of $UO_2$ fuels at high burn-up, Journal of Nuclear Materials, Vol. 346, pp. 131-144.

Turnbull J.A., Friskney C.A., Findlay J.R., Johnson F.A., Walter A.J. (1982). The diffusion coefficients of gaseous and volatile species during the irradiation of uranium oxide, Journal of Nuclear Materials, Vol. 107, pp. 168-184.

Turnbull J.A., White R.J., Wise C.A. (1988). The diffusion coefficient for fission gas atoms in uranium dioxide, Proceedings of Technical Committee Meeting on Water Reactor Fuel Element Computer Modelling in Steady State, Transient and Accidental Conditions, Preston, England, September 18-22, 1988.

Van Uffelen P., Schubert A., van de Laar J., Győri C., Elenkov D., Boneva S., Georgieva M., Georgiev S., Hózer Z., Märtens D., Spykman G., Hellwig C., Nordstrøm Å., Luzzi L., Di Marcello V., Ott L. (2007). The verification of the TRANSURANUS fuel performance code - an overview, INRNE (Ed.), Proceedings of 7th International Conference on WWER Fuel Performance, Modelling and Experimental Support, Albena, Bulgaria, 17-21 September, 2007, pp. 305-320.

Van Uffelen P., Schubert A., van de Laar J., Győri C (2008). Development of a Transient Fission Gas Release Model for TRANSURANUS, Proceedings of the Water Reactor Fuel Performance Meeting (WRFPM - Top Fuel 2008), Seoul, Korea, October 19-23, 2008.

Veshchunov M.S. (2008). Modelling of grain face bubbles coalescence in irradiated $UO_2$ fuel, Journal of Nuclear Materials, Vol. 374, pp. 44-53.

White R.J. (1994). A new mechanistic model for the calculation of fission gas release, Proceedings of the International Topical Meeting On Light Water Reactor Fuel Performance, West Palm Beach, Florida, USA, April 17-21, 1994.

White R.J. (2004). The development of grain-face porosity in irradiated oxide fuel, Journal of Nuclear Materials, Vol. 325, pp. 61-77.

White R.J., Tucker M.O. (1983). A new fission-gas release model, Journal of Nuclear Materials, Vol. 118, pp. 1-38.

White R.J., Corcoran R.C., Barnes J.P. (2006). A Summary of Swelling Data Obtained from the AGR/Halden Ramp Test Programme, Report R&T/NG/EXT/REP/0206/02, 2006.

(This page has been intentionally left blank)

## APPENDIX

In this Appendix, the equation used in the present model for describing the coalescence process of intra-granular gas pores – Eq. (1.26) – is derived.

The geometrical reasoning proposed by White (2004) and discussed in subsection 1.3.3 entails that the total rate of loss of gas pores by coalescence following an increase in the (mean) pore area due to bubble growth, $(dA_{gp})_g$, is given by (White 2004):

$$dN_{gp} = -2N_{gp}^2 \left(dA_{gp}\right)_g , \tag{A.1}$$

or:

$$\frac{dN_{gp}}{dt} = -2N_{gp}^2 \left(\frac{dA_{gp}}{dt}\right)_g , \tag{A.2}$$

where $(dA_{gp}/dt)_g$ denotes the variation of the pore area owing solely to bubble growth. White assumed that the newly coalesced pore retains the same area of the two individual parent pores. Differently, in the present model, the total volume (summation of the volumes of the single pores) per unit grain boundary area is assumed to be conserved through coalescence, i.e., the volume of the newly coalesced pore equals the sum of the volumes of the two individual parent pores.
Given that the pore density, $N_{gp}$, decreases through coalescence, the conservation of the total pore volume per unit grain boundary area, $N_{gp}V_{gp}$, implies a variation of the average pore volume, $V_{gp}$, due to coalescence. As a result, the total rate of increase in the average pore volume may be expressed as:

$$\frac{dV_{gp}}{dt} = \left(\frac{dV_{gp}}{dt}\right)_g + \left(\frac{dV_{gp}}{dt}\right)_c , \tag{A.3}$$

where $(dV_{gp}/dt)_g$ denotes the variation of the pore volume owing solely to bubble growth, and $(dV_{gp}/dt)_c$ the variation of the average pore volume owing solely to coalescence. The variation of the total pore volume per unit grain boundary area is due solely to pore growth and may be expressed as:

$$\frac{d\left(N_{gp}V_{gp}\right)}{dt} = N_{gp}\left(\frac{dV_{gp}}{dt}\right)_g , \tag{A.4}$$

where

$$\frac{d\left(N_{gp}V_{gp}\right)}{dt} = N_{gp}\frac{dV_{gp}}{dt} + V_{gp}\frac{dN_{gp}}{dt} . \tag{A.5}$$

Superposition of Eqs. (A.3), (A.4) and (A.5) yields:

$$\left(\frac{dV_{gp}}{dt}\right)_c = -\frac{V_{gp}}{N_{gp}}\frac{dN_{gp}}{dt} , \tag{A.6}$$

Given that $V_{gp} \sim A_{gp}^{3/2}$, Eq. (A.3) implies:

$$\frac{dA_{gp}}{dt} = \left(\frac{dA_{gp}}{dt}\right)_g + \left(\frac{dA_{gp}}{dt}\right)_c, \tag{A.7}$$

where $(dA_{gp}/dt)_c$ denotes the variation of the average pore area owing solely to coalescence, and Eq. (A.6) can be written in terms of average pore area as:

$$\left(\frac{dA_{gp}}{dt}\right)_c = -\frac{2}{3}\frac{A_{gp}}{N_{gp}}\frac{dN_{gp}}{dt}, \tag{A.8}$$

Combining Eqs. (A.2), (A.7) and (A.8), one obtains for the total rate of loss of pores by coalescence according to the present model:

$$\frac{dN_{gp}}{dA_{gp}} = -\frac{6N_{gp}^2}{3+4N_{gp}A_{gp}} \tag{1.26}$$

(This page has been intentionally left blank)

(This page has been intentionally left blank)